Coordination Chemistry Reviews 254 (2010) 331–345

Contents lists available at ScienceDirect

Coordination Chemistry Reviews

journal homepage: www.elsevier.com/locate/ccr

Review

Inter- or intramolecular electron transfer between triruthenium clusters: we'll cross that bridge when we come to it

Starla D. Glover[a], John C. Goeltz[a], Benjamin J. Lear[b], Clifford P. Kubiak[a,*]

[a] Department of Chemistry & Biochemistry, University of California, San Diego, 9500 Gilman Drive, Mail Code 0358, La Jolla, CA 92093, United States
[b] Department of Chemistry, The Ohio State University, 100 West 18th Avenue, Columbus, Ohio 43210-1185, United States

Contents

ARTICLE INFO

Article history:
Received 8 April 2009
Accepted 6 September 2009
Available online 11 September 2009

Keywords:
Mixed valence
Electron transfer
Spectroelectrochemistry
Self-exchange
Ruthenium

ABSTRACT

The purpose of this review is to examine the fundamental differences between intermolecular self-exchange vs. intramolecular ET in mixed-valence complexes based on similar triruthenium structural units. The role of orbital overlap between ancillary ligands of the electron donor and acceptor are considered in self-exchange reactions which are found to be strongly adiabatic and again in bridged mixed-valence systems. The method of infrared (IR) reflectance spectroelectrochemistry for the determination of extremely fast (10^{11}–10^{13} s^{-1}) ET rate constants is reviewed as a tool to provide quantitative information about the time scales of localization and delocalization. The role of internal vibrations of the bridging ligand in strongly delocalized mixed-valence ions is investigated by resonance Raman and IR spectroscopies. The role of solvent dipolar relaxation times in determining the rates of ultrafast intramolecular ET reactions is reviewed in the context of inorganic mixed-valence chemistry. Finally, the concept of Robin–Day Class II/III "borderline" complexes is considered, and a concise definition of the localized to delocalized transition is provided in terms of the relative contributions of external solvent and internal complex ion vibrational modes to ET.

1. Introduction

Electron transfer (ET) is not only the simplest reaction in the field of coordination chemistry, but also the most important as all life processes and many technologies depend on it. In this review, we consider 12 years of work on intramolecular electron transfer (ET) reactions within mixed-valence ions of the general type $[Ru_3O(OAc)_6(L)(CO)(\mu\text{-BL})Ru_3O(OAc)_6(L)(CO)]^-$ (L = pyridyl or isocyanide ligand; BL = 4,4′-bipyridine or pyrazine) [1–21]. There are two key concepts that we wish to discuss and illustrate with examples from our work. The first is the fundamental difference between intermolecular self-exchange and intramolecular electron transfer through a donor-bridge-acceptor assembly. The second concept is the localized to delocalized transition, the transition that occurs at the borderline between Robin–Day [22] Class II and Class III systems [23]. We will take the liberty of not presenting the work in a historical sequence, but will begin by considering some of our more recent work on electron self-exchange reactions of the ruthenium clusters of the type $[Ru_3O(OAc)_6(L)_2(CO)]$ (Fig. 1) which constitute "half" of the dimer of trimer mixed-valence ions (Fig. 12) [21]. Our intent here is to determine the rates of self-exchange, individual cluster reorganization energies, and general features that will shed light on the unusual intramolecular ET properties of the pyrazine-bridged mixed-valence ions that are based on the same structural and redox unit. We will then move on to consider these latter systems in which the electron donor and acceptor are covalently joined by a pyrazine or similar bridging ligand. We will review the importance

* Corresponding author. Tel.: +1 858 822 2665; fax: +1 858 822 4442.
E-mail address: ckubiak@ucsd.edu (C.P. Kubiak).

0010-8545/$ – see front matter © 2009 Elsevier B.V. All rights reserved.
doi:10.1016/j.ccr.2009.09.005

of energetic alignment of donor-bridge-acceptor triad, the importance of bridging ligand modes of vibration as probed by resonance Raman and IR spectroscopies, and the role of solvent dynamics in controlling the rates and degrees of localization/delocalization in very rapidly exchanging Class II/III borderline systems.

2. Self-exchange—take the bridge or the tunnel?

Within the context of the Marcus–Hush theory of electron transfer (ET) [24,25], rates of electron self-exchange can be related directly to the total reorganization energy for ET, λ, and by the Marcus cross relation, to rates of intermolecular ET with other redox agents [26,27]. Here, we examine the self-exchange ET reactions of ruthenium clusters of the type $[Ru_3O(OAc)_6(CO)(L)_2]$ (Fig. 1) which constitute "half" of the dimer of trimer mixed-valence ions discussed in more detail later in this review. We will show examples of *inter*molecular electron exchange reactions that are best described as coupled systems that are strongly adiabatic.

The three different ancillary pyridine ligands used dictate the redox potentials of the clusters, as shown in Fig. 2. The redox events are typically discussed as metal cluster-based, with the reduction of the neutral complex to the monoanion at around −1500 mV vs. the ferrocene/ferrocenium couple, corresponding formally to the reduction of $Ru^{III}Ru^{III}Ru^{II}$ to $Ru^{III}Ru^{II}Ru^{II}$. As can be seen, the redox potential is sensitive to the identity of the ancillary pyridyl ligand (specifically the pK_a of the conjugate acid). An initial question then is how the intermolecular ET rate for electron exchange between the neutral and anionic species in solution depends on changes in the ancillary ligands.

This question was answered using a standard NMR kinetic study [28], in which the shifts and line broadening in ^{1}H NMR signals were examined as a function of the concentrations and mole fractions of the neutral and reduced clusters to determine rate constants for self-exchange. The mole fractions of diamagnetic neutral clusters and paramagnetic singly reduced clusters in solution were initially determined by IR spectroscopy, by integration of the ν(CO) bands for the neutral cluster (~1940 cm^{-1}) and the singly reduced cluster (~1900 cm^{-1}). Spectra for **1** in CD_2Cl_2 are shown in Fig. 3(a). The ν(CO) region for the mixed solutions was not coalesced and could be fit to two well resolved bands, giving an upper bound to k_{ET} of ~10^{10}–10^{11} s^{-1} M^{-1} [11]. However, the exchange was in the fast regime on the NMR timescale (where $k(C_{tot}) \gg 2\pi(\Delta\nu)$),

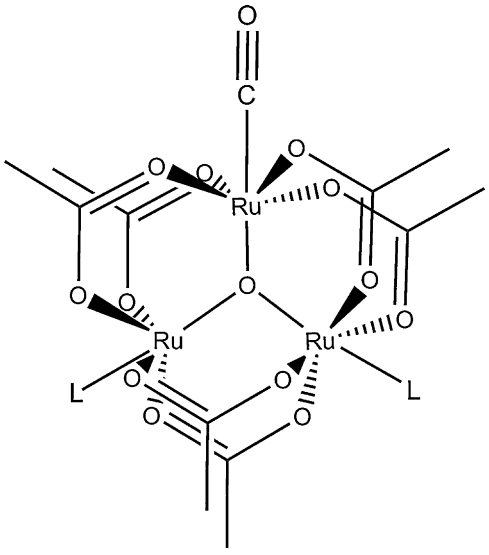

Fig. 1. The three clusters used in Section 1: **1**, L = 4-cyanopyridine (cpy); **2**, L = pyridine (py); **3**, L = 4-(dimethyl)aminopyridine (dmap) [21].

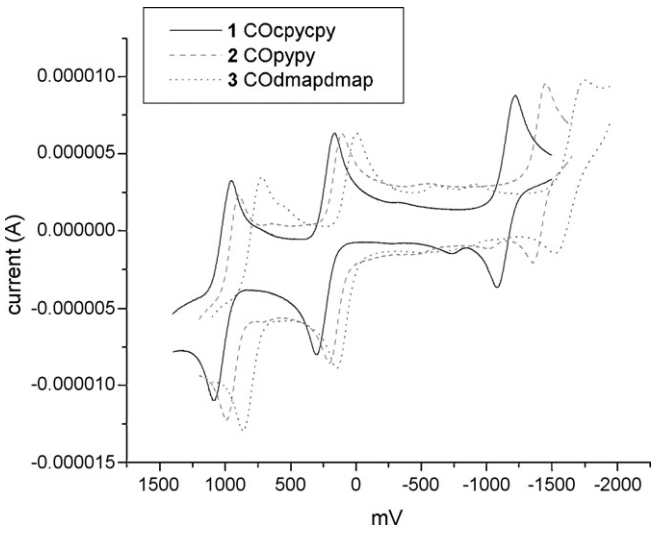

Fig. 2. Electrochemistry of ruthenium trimers with different pyridyl ligands in CH_2Cl_2 with 0.1 M TBAH, glassy carbon working, platinum wire counter, and Fc/Fc^+ reference electrodes [21].

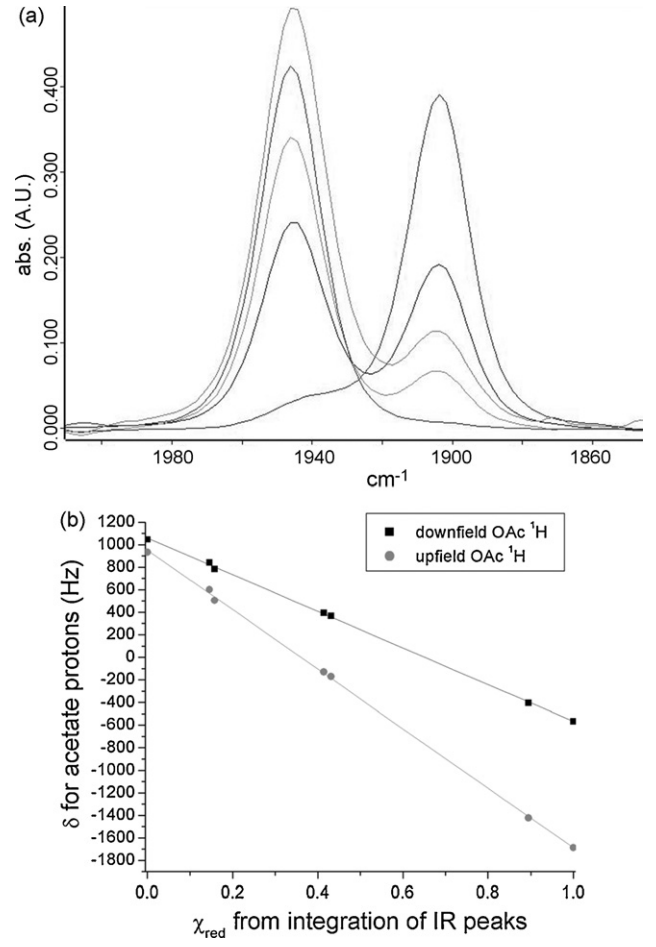

Fig. 3. (a) IR spectra of the ν(CO) region for **1** in CD_2Cl_2, with varying mole fractions, χ_{red}, of [red]/[ox]. (b) Plot of χ_{red} determined from integration of IR peaks vs. chemical shift of acetate protons [21]. The linear relationship confirms fast exchange on the NMR timescale.

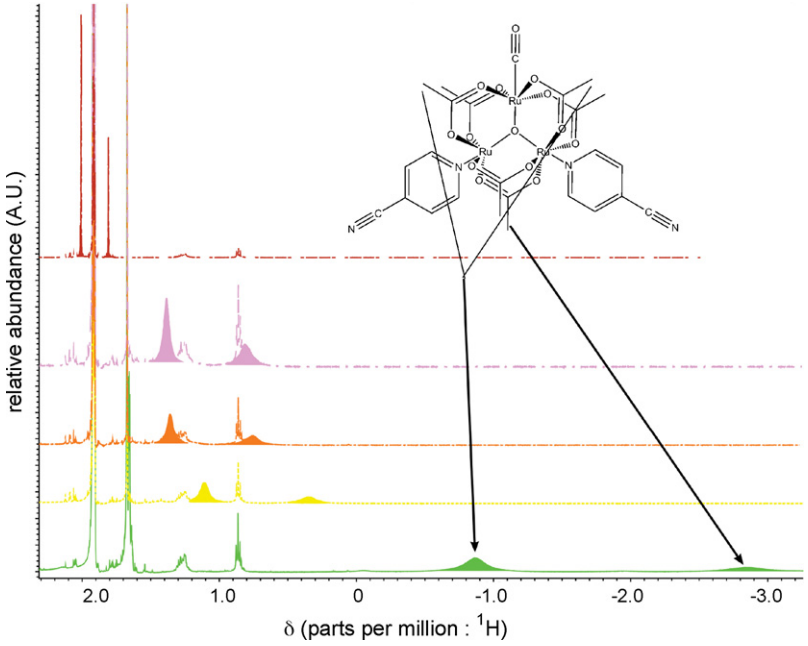

Fig. 4. Representative ^{1}H NMR spectra with varying mole fractions of diamagnetic and paramagnetic $\mathbf{1}^{0/-}$ in CD_3CN [21].

as the chemical shifts for exchanging species were averages of the diamagnetic and paramagnetic chemical shifts, weighted by their respective mole fractions. This is shown in the linear relationship in the mole fraction of reduced complex (determined by IR) vs. acetate chemical shift in Fig. 3(b).

Rate constants were determined using the Equation (1) below:

$$k_{ET} = \frac{4\pi\chi_d\chi_p(\Delta\nu)^2}{(W_{dp} - \chi_p W_p - \chi_d W_d)C_{tot}} \quad (1)$$

where χ_d and χ_p are the mole fractions of diamagnetic and paramagnetic species, $\Delta\nu$ is the difference in chemical shift between diamagnetic and paramagnetic species in Hz, W_{dp} is the peak width at half maximum for the mixture in question, W_d and W_p are the widths for the pure diamagnetic and paramagnetic species, and C_{tot} is the total concentration in mol L^{-1} [28]. Representative NMR spectra for **1** in CD_3CN are shown in Fig. 4. The rate constants measured range from 10^6 to 10^8 s^{-1} M^{-1} and are shown in Table 1. These rate constants are comparable in magnitude to those found by NMR line broadening methods for many other 0/+ and 0/− couples,

Table 1
Electron-transfer rate constants ($\times 10^7$ s^{-1} M^{-1}) [21].

	CD_3CN	THF-d_8	CD_2Cl_2
1 COcpycpy	13	20	30
2 COpypy	1.8	20	7
3 COdmapdmap	0.7	2	–

though the range seen here of more than an order of magnitude of difference between **1** and **3** is remarkable for analogous self-exchange couples [29–34]. In a particularly relevant study reported by Meyer, $Ru_3O(OAc)_6(py)_3^{0/+}$ exhibited $k_{ET} = 1.1 \times 10^8$ s^{-1} M^{-1} in CD_2Cl_2 [30].

Looking at the observed k_{ET} for complexes **1**–**3**, one trend is immediately clear: more electron withdrawing substituents on the ancillary pyridine ligands promotes faster self-exchange in all three solvents. We attribute this to increasing donor–acceptor orbital overlap, or "contact area," as more electron density is drawn onto the pyridine ligands of the $[Ru_3O(OAc)_6(CO)(L)_2]^-$ donor. This is depicted schematically in Fig. 5 as simple overlap integrals repre-

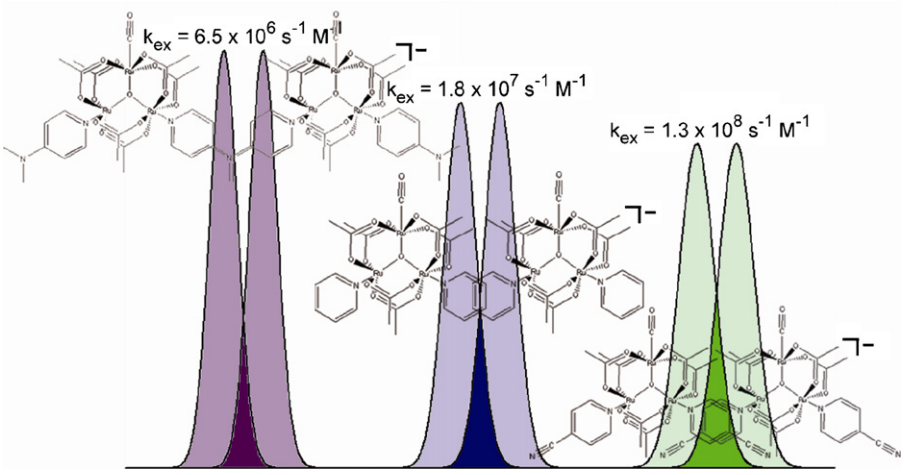

Fig. 5. Schematic depiction of increased overlap leading to increased coupling and rates of self-exchange.

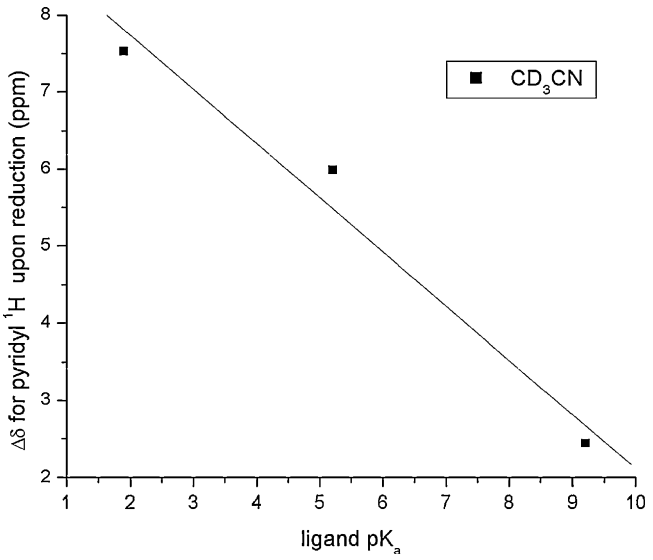

Fig. 6. Plot of ligand pK_a vs. the average change in chemical shift ($\Delta\delta$) for the pyridyl protons upon reduction of the neutral cluster in CD_3CN [21].

senting the trend in electron exchange coupling, H_{AB}, according to the Wolfsburg–Helmholtz–Mulliken approximation [35].

One set of observations in support of the orbital overlap description is a strong correlation between k_{ET} and the amount of unpaired electron spin density on the ancillary pyridine ligands. Average $\Delta\delta s$ for pyridyl protons in the three complexes and their reduced counterparts in CD_3CN are shown in Fig. 6. As the pyridine ligand becomes less basic (lower pK_a) more electron density is drawn onto the ring in the reduced cluster, and the contact shift is greater.

A logarithmic plot of k_{ET} vs. ligand pK_a is linear (Fig. 7), suggesting that the electron withdrawing nature of the ligands and thus the effective contact area factors into the activation energy for ET. To the best of our knowledge, a simple quantitative proxy for orbital overlap has never before been correlated with observed rates of electron self-exchange, even though orbital overlap has been invoked previously to explain the difference in self-exchange rate constants for the ferrocene/ferrocenium ($Fc^{0/+}$) and cobaltocene/cobaltocenium ($Cc^{0/+}$) couples [31]. In that case, the main difference is that the Fc orbital in question is iron-based, whereas in Cc the orbital is spread over more of the molecule.

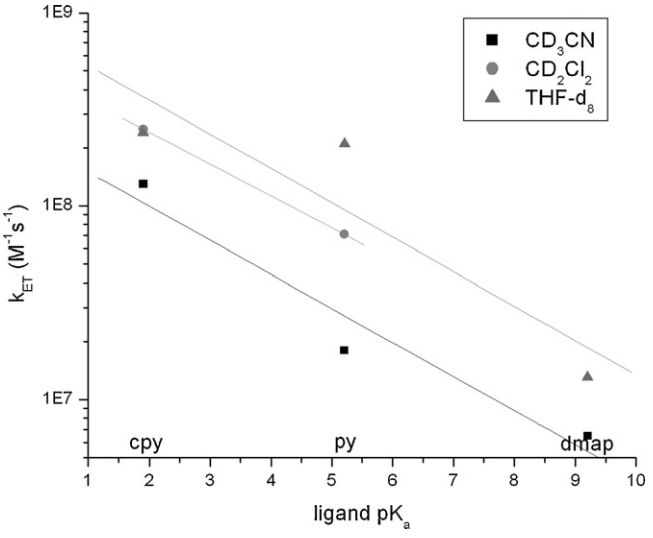

Fig. 7. Plot of ln(k_{ET}) vs. ligand pK_a with linear fits. The linear relationship indicates that pK_a is a good proxy for the amount of electron density on the pyridine ligand in the reduced state and thus the donor–acceptor orbital overlap, which figures into the activation barrier to ET [21].

The orbital overlap description of ET we invoke here to describe these self-exchange reactions differs substantially from the frequently invoked tunneling model. Fig. 8 depicts two diabatic potential energy surfaces with important vibrational wave functions within the electronic states. Vibrational wavefunction overlap between the adjacent electronic states provides a mechanism for electron tunneling from one diabatic electronic state to the other. Because the symmetry of the $\nu = 0, 1, 2$, etc. vibrational wave functions only provides good overlap in the vibrational excited states (where they have significant probability density at the classical turning points), low frequency modes of vibration will be the most likely to contribute to the tunneling ET pathway. Rates of ET will be influenced strongly by the energy placement within the potential energy surface and slope of the surface. The placement of these specific vibrational levels within each potential energy surface can be modified by ligand substitution and other factors that change the electronic and vibrational structure of a donor/acceptor pair.

There are several reasons why we favor a strongly adiabatic orbital overlap model for ET compared to the diabatic tunneling model for the self-exchange reactions being considered here. For the three pyridine ligands used in this study, the pyridine skeletal modes (e.g. 1581 cm^{-1}) change by less than 1.5% from 4-cyanopyridine to 4-(dimethylamino)pyridine. Lower frequency cluster skeletal modes in the vicinity of the point of substitution can be expected to change by no more than this. Monoanionic pyrazine bridged dimers of these clusters exhibit picosecond ground state ET, and the reorganization energy, λ, for the pair of exchanging clusters has been estimated at 1.25 eV, or 10,000 cm^{-1} [4,16]. Rate constants on the picosecond time scale and reorganization energies on the order of 1 eV can only be reconciled by very large electronic couplings, H_{AB}, that drive the activation energy towards zero. This is best explained by strong electronic delocalization owing to strong donor-bridge-acceptor orbital overlap. Essentially, the clear evidence of significant and increasing unpaired electron spin density on the peripheral pyridine ligands of the anions of **1**, **2**, and **3** as the rate of ET increases, combined with the fact that replacing one of the pyridine ligands with a bridging pyrazine produces strongly delocalized mixed-valence ions, provides a consistent physical model for explaining rates of ET in both the intermolecular self-exchange and intramolecular mixed-valence limits. We conclude that intermolecular electron transfer studied here must be in the adiabatic regime with H_{AB} on the order of 10–20% of the reorganization energy λ to achieve the observed rates on the order of 10^8 s^{-1} as estimated from the following widely used equation (Eq. (2)) using estimates of λ on the order of 1 eV [36]. This is depicted graphically in Fig. 9, where the Marcus equation is used to predict k_{ET} in terms of H_{AB}/λ for several reasonable values of λ. Different values are plotted to show that our analysis holds true at different val-

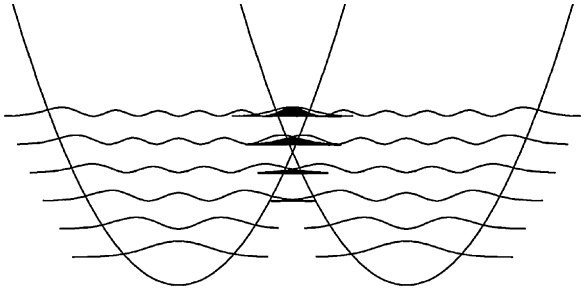

Fig. 8. Probability functions for vibrational energy levels, $\nu = 0$–5. Areas of overlap with increased probability of tunneling between electronic states are shaded.

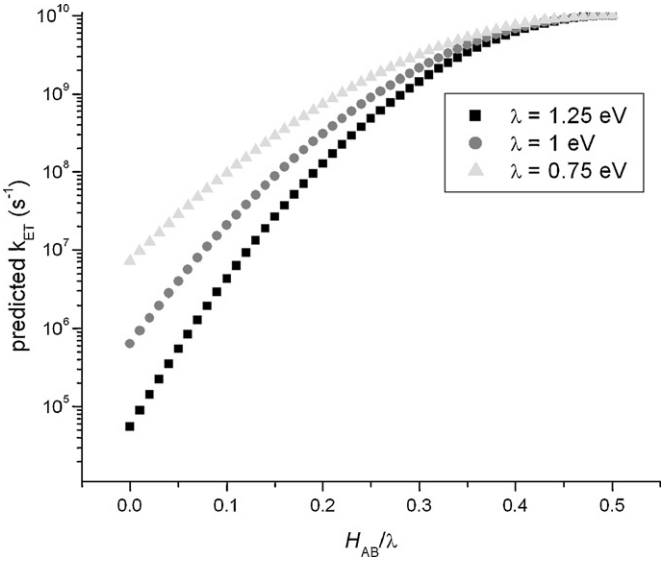

Fig. 9. Plot of predicted [36] k_{ET} vs. H_{AB}/λ. H_{AB} must be a significant fraction of λ to achieve the observed rate constants of 10^6–10^8 s^{-1}, placing the intermolecular ET in the adiabatic regime.

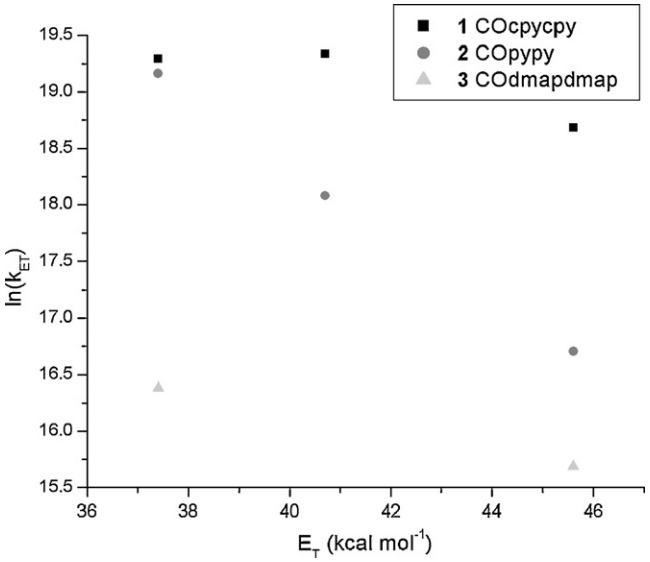

Fig. 11. Plot of ln(k_{ET}) vs. solvent microscopic polarity, E_T. Values of E_T = 37.4, 40.7, and 45.6 kcal mol^{-1} correspond to THF, CH_2Cl_2, and CH_3CN, respectively [21].

ues of λ, not to indicate any expected differences in reorganization energy between clusters **1**–**3**:

$$k_{ET} = \kappa\nu \exp\left[-\frac{((\lambda/4) - H_{AB} + (H_{AB}^2/\lambda))}{RT}\right] \quad (2)$$

With respect to outer sphere thermodynamic solvent parameters, **1**–**3** behave normally. A log plot of k_{ET} vs. the solvent variable portion of the outer sphere reorganization energy [4] $(1/\varepsilon_{op} - 1/\varepsilon_s)$ shows that self-exchange is slower with increasing outer sphere solvent reorganization energy (Fig. 10). The observed rate constants also correlate well with solvent microscopic polarities [4], slowing with increasing E_T (Fig. 11).

These results add to the quantitative understanding of electron self-exchange reactions. We were able to correlate the electron withdrawing ability of ancillary ligands to intermolecular electron-transfer rate constants. A plot of ln(k_{ET}) vs. the pyridine ligand pK_a is linear, suggesting that donor–acceptor orbital overlap is a major contributor to the ET activation barrier. A greater ^{1}H NMR contact shift for the pyridyl protons indicates increased electron spin density on ancillary pyridine ligands with more electron withdrawing groups. This leads to an increase in H_{AB}, the matrix element that describes the mixing of the two wavefunctions involved in electron exchange, which in turn reduces the barrier to ET.

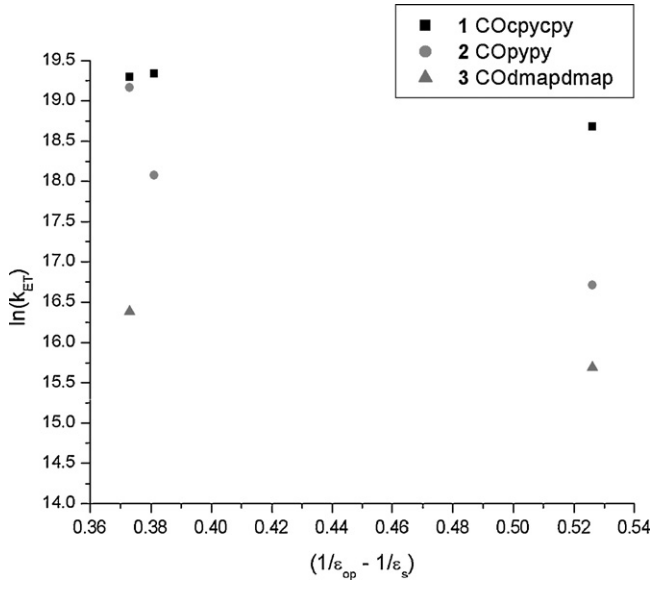

Fig. 10. Plot of ln(k_{ET}) vs. $(1/\varepsilon_{op} - 1/\varepsilon_s)$. Values of $(1/\varepsilon_{op} - 1/\varepsilon_s)$ = 0.373, 0.381, and 0.525 correspond to THF, CH_2Cl_2, and CH_3CN, respectively. The rate decreases with increasing outer sphere solvent reorganization energy [21].

This work also underscores the general importance of metal cluster orbital extension onto ligands. Often it is assumed that an oxidation state or a redox event is localized on a metal center or cluster. On the contrary, the delocalization of charge onto peripheral ligands is shown in this work to play an important role in ET. The effect here is so strong that by simple variation of the pyridine ligands, rate constants can be varied by almost two orders of magnitude for a reaction with zero thermodynamic driving force. In addition, this drives home the fact that in the adiabatic regime orbital overlap has a strong influence on k_{ET}—a result that should be unsurprising considering the fact that adiabaticity (strong coupling) by definition requires wavefunction mixing.

3. When you come to a bridge on the road, take it

The presence and transfer of electron spin density on the pyridine ligands in the self-exchange reactions described in the previous section illustrates how $[Ru_3O(AcO)_6(CO)(L)_2]$ units contribute to very strongly interacting mixed-valence ions when they are bridged by pyrazine [9]. Pyrazine is an even more effective electron withdrawing pyridyl ligand (with a pK_a ~1) compared to the three pyridines employed in the self-exchange study. It would be expected then that delocalization of electron density onto the pyrazine bridge would be preferred, promoting electron transfer to the other Ru_3 cluster, and contributing to inter-cluster electron transfer and delocalization. This also helps explain why the fastest exchange times are observed for dimers with electron donating and aliphatic ancillary ligands, which do not have low lying π* orbitals to accept electron density from the reduced cluster in competition with the bridging pyrazine [19].

Dimers of the trinuclear ruthenium clusters form stable charge-transfer complexes with overall −1 charge, and undergo rapid intramolecular electron transfer between the coupled Ru_3 clusters when bridged by pyrazine (pz) or 4,4′-bipyridine (bpy) [10].

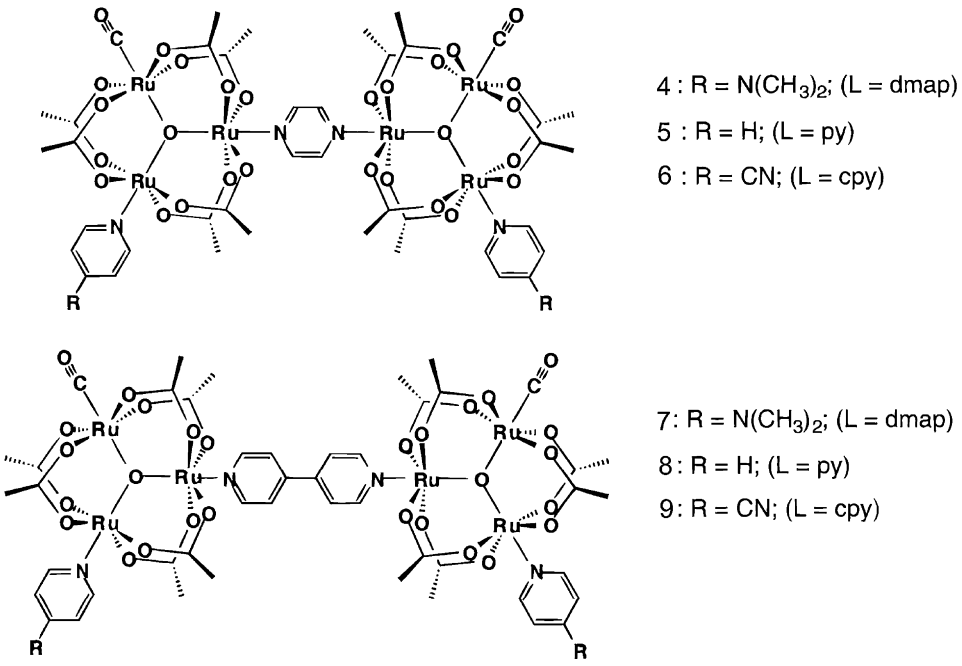

Fig. 12. Dimers of ruthenium trimers with bridging ligand = pyrazine (**4**–**6**) or 4,4′-bipyridine (**7**–**9**) and varying ancillary ligands [10].

The dimers **4**–**9** discussed here are shown in Fig. 12. In contrast to the single electron processes seen in the electrochemistry of the "monomers" in Fig. 2, the dimers show concerted two electron oxidations, but two single electron cathodic processes that formally generate $Ru_3^{III,III,II}$–BL–$Ru_3^{III,II,II}$ (0/−1) and subsequently $Ru_3^{III,II,II}$–BL–$Ru_3^{III,II,II}$ (−1/−2). The varied splittings qualitatively indicate the varying degrees of inter-cluster electronic communication that is dependent on the identity of both the bridging ligand and ancillary ligands [10].

In the case of **4**, ΔE = 440 mV, which corresponds to a comproportionation constant, $K_c = \exp(\Delta EF/RT) = 2.7 \times 10^7$ for the stability of the monoanionic mixed-valence complex relative to the isovalent neutral complex and the dianion. The relationship between the electrochemical value of ΔE and the electronic coupling, H_{AB}, has been discussed [10,37–40], and though many factors are involved, increased ΔE tends to indicate greater electronic coupling for analogous complexes under similar conditions. An interesting aspect of these complexes is that the splitting, ΔE, between the (0/−1) and (−1/−2) states of **4**–**9** depends strongly on the ancillary ligands (dmap, py, cpy) and on the bridging ligand (pz, bpy). Indeed the comproportionation constant K_c falls by three orders of magnitude across the pz bridged dimers **4**–**6** and falls to a value of less than 10 for the most weakly coupled system **9** (Fig. 13). Data are presented in Table 2.

While remote ligand control of electronic coupling in mixed-valence complexes is not unusual [37,41,42], the wide variation achieved here by simple substitution of bridging and ancillary ligands is remarkable. It appears that two conditions are simultaneously met: (i) very favorable overlap between the Ru_3 cluster dπ-electron system and the bridging pz or bpy π* system, and (ii) the ability to raise or lower the energy of the Ru_3 cluster d-electron levels engaging the pz or bpy π* system by changing the electron donor/acceptor ability of the ancillary pyridyl ligand. The relevant Ru d level is then closer to the pz π* level in **4** than in **6**, and closer to the bpy π* level in **7** than in **9**. It is worth keeping in mind the NMR kinetics study discussed above, particularly the pyridyl contact shifts, as the energetic matching effect (ii) may be convoluted with a simultaneous push–pull effect where electron donating ancillary ligands push excess electron density onto the bridge more effectively than electron withdrawing ancillary ligands. Three lines of experimental evidence support this description of the electronic structure: (a) the metal-to-ligand charge transfer (MLCT) absorptions for the Ru d to π* transitions appear at increasing energies in the series **4**–**6** (482, 475, and 450 nm, respectively); (b) the average of the reduction potentials $E_{1/2}(0/-1)$ and $E_{1/2}(-1/-2)$ becomes more positive in the series **4**–**6** and **7**–**9**, and (c) the same type of Ru_3 clusters bridged by 1,4-diazabicyclo[2.2.2]octane (dabco), which has no π-electron system, show no electronic coupling, i.e. ΔE = 0.

The ΔE values for the bpy bridged complexes **7**–**9** are approximately 25% of the values for the pz bridged complexes **4**–**6** with the same pyridyl ligands. In general, electronic coupling falls off exponentially with distance between electronically interacting centers [39]. The longer separation in **7**–**9** decreases the intercluster electronic coupling, thereby decreasing ΔE values and calculated comproportionation constants.

To assess further the extent of electronic interaction between the two coupled Ru_3 units in the −1 states, intervalence charge transfer (IVCT) spectra were examined. Fig. 14 shows the electronic absorption spectra of the −1 states of **4**–**6**. The lowest energy absorption is assigned to intracluster excitation because it also appears in the −2 state with about double the extinction coefficient, albeit blue-shifted somewhat in energy, and appears in the non-bridged clusters with one CO and two pyridyl ligands in the −1 state. The middle band at 11,000–12,000 cm^{-1} is then assigned to the intervalence charge transfer absorption. Though in some cases the peaks do not fit well to a single Gaussian function, this is not unexpected [36] and the Gaussian that generally describes

Table 2
Electrochemical data for $[Ru_3(\mu_3\text{-}O)(\mu\text{-}OAc)_6(CO)(L)]_2(\mu\text{-}BL)$ in CH_2Cl_2.

	BL	L	$E_{1/2}(0/-1)$, V	$E_{1/2}(-1/-2)$, V	ΔE (mV)	K_c
4	pz	dmap	−0.89	−1.33	440	2.7×10^7
5	pz	py	−0.81	−1.19	380	2.7×10^6
6	pz	cpy	−0.68	−0.93	250	1.7×10^4
7	bpy	dmap	−1.11	−1.23	120	1.1×10^2
8	bpy	py	−1.03	−1.11	80	2.3×10^1
9	bpy	cpy	−0.91	−0.91	<50	<10

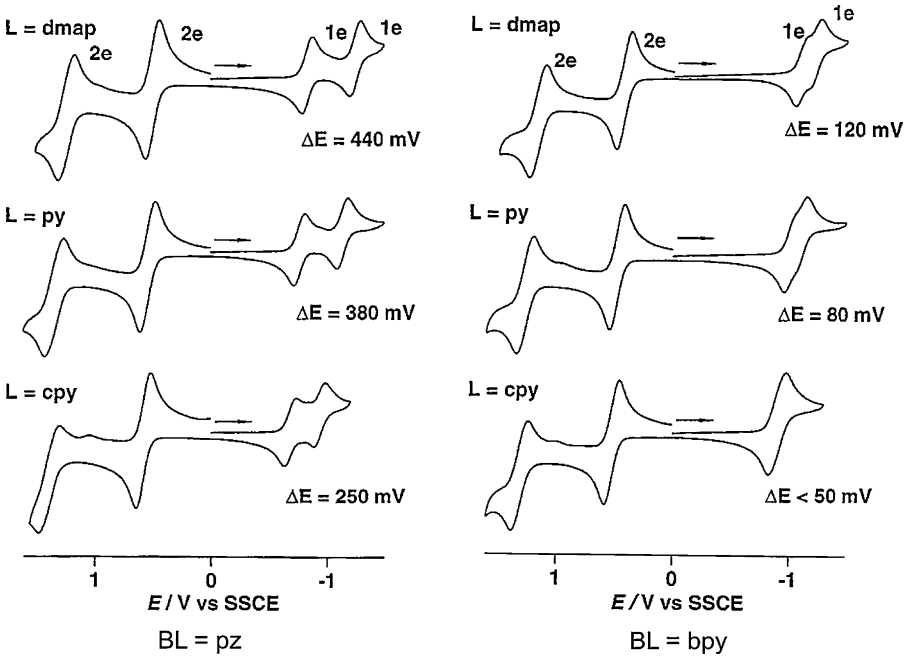

Fig. 13. Electrochemistry of dimers **4**–**9**, ~1 mM in CH_2Cl_2, with 0.1 M Bu_4NPF_6 supporting electrolyte, glassy carbon WE, Pt wire CE, and SSCE reference electrode, at a scan rate of 100 mV/s [10]. The anodic peaks are two electron oxidations, attributed to concurrent one electron oxidations of each Ru_3 cluster. The cathodic peaks are one electron reductions, with splittings indicative of electronic communication between the two bridged Ru_3 clusters, as discussed in greater detail later in the review.

the bandshape is still indicative of the energy and allowedness of the transition.

The details of the observed IVCT bands and the calculated values for H_{AB} using the two-state Hush model [24] are summarized in Table 3. While the electron transfer distances used to calculate H_{AB} are only estimates, the assumption that the IVCT bandshape should consist of a single Gaussian may not be correct, and more recent studies indicated significantly larger absolute values for H_{AB} [16], the *relative* values for electronic coupling calculated from the optical spectra are still instructive. In good agreement with the electrochemical data, electronic spectra indicated decreasing electronic coupling in the series **4**–**6**. The IVCT band positions shift from higher to lower energies, the band intensities decrease, and the bands broaden, all indicating decreased coupling [36]. This analysis will be discussed in greater detail in a section below with regard to resonance Raman studies of pyrazine bridge vibrational modes.

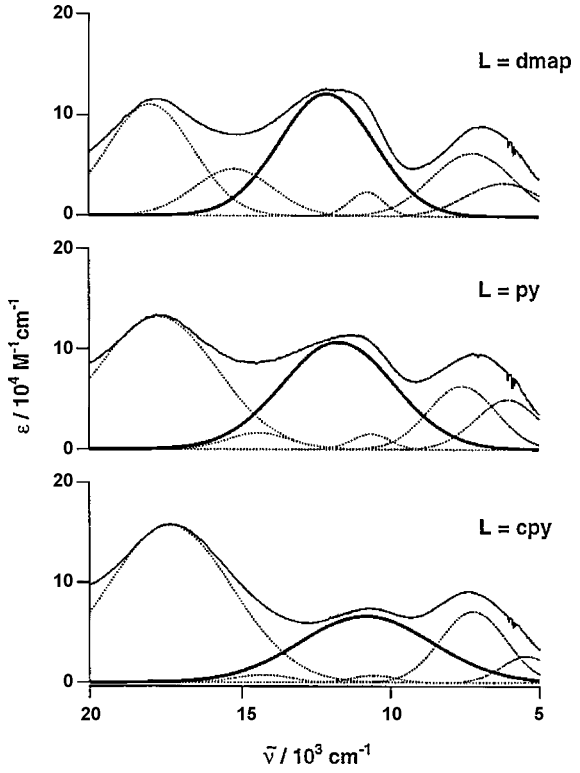

Fig. 14. Electronic absorption spectra for $\mathbf{4}^-$–$\mathbf{6}^-$ (top to bottom) in CH_2Cl_2 with 0.1 M Bu_4NPF_6, fit to multiple Gaussian bands [10]. Note that the energy and intensity of the intervalence charge transfer band (ca. 11,000–12,000 cm^{-1}) decrease in the series **4**–**6** indicating a decrease in electronic coupling.

The vibrational spectra of complexes **4**–**9** were obtained using reflectance IR spectroelectrochemistry (SEC). Controlled potentials were applied to prepare the singly (−1) and doubly (−2) reduced states of each complex. The normal modes associated with C–O stretching of the carbon monoxide ligands on each $Ru_3^{III,III,II}$ unit contribute to a single ν(CO) band due to their identical environments and large spatial separation, and result in a single well defined peak at ~1940 cm^{-1} for the neutral complexes and at ~1890 cm^{-1} in the doubly reduced complexes. In view of these results and the well resolved peaks seen in partly reduced solutions of the monomer clusters **1**–**3** (Fig. 3a) it is reasonable to expect two peaks at 1940 and 1890 cm^{-1} in the −1 bridged clusters. Indeed in the bpy bridged clusters **7**–**9** this is observed, with only mild broadening in **7**, as shown in Fig. 15.

However in the mixed-valence −1 states of **4**–**6**, two resolved ν(CO) bands are not observed. In the case of $\mathbf{4}^-$, one broad band is seen at the average of the neutral and doubly reduced band maxima (Fig. 16, top). The degree of "coalescence" of the IR spectra depends

Table 3
Summary of electronic spectral data for the IVCT bands of the mixed-valence (−1) state of $[Ru_3(\mu_3\text{-}O)(\mu\text{-}OAc)_6(CO)(L)]_2(\mu\text{-}pz)$ [10].

	L	ν_{max} (cm^{-1})	ε_{max} ($M^{-1}\,cm^{-1}$)	$\Delta\nu_{1/2}$ (cm^{-1})	H_{AB} (cm^{-1}) from two state model [24]
4	dmap	12,100	12,200	3760	2180
5	py	11,800	10,700	3920	2060
6	cpy	10,800	6,610	5220	1310

on the rate of electron transfer between the pyrazine-linked Ru_3 clusters. **5** and **6** exhibited less coupling in their electrochemical and optical responses, and exhibit less coalesced ν(CO) bands in the mixed-valence state. Bloch-type line shape analysis developed by McClung and co-workers [43] can be used to simulate IR spectra obtained from exchanging species and is used to estimate rates of electron transfer. Rates estimated for $\mathbf{4}^-$, $\mathbf{5}^-$, and $\mathbf{6}^-$ are $9 \pm 3 \times 10^{11}$, $5 \pm 3 \times 10^{11}$, and ca. 1×10^{11} s^{-1}, respectively, in CH_2Cl_2 with 0.1 M Bu_4NPF_6. A rate for $\mathbf{7}^-$ can also be estimated at ca. 1×10^{11} s^{-1}, though as is clearly visible in the spectrum (Fig. 15, top) the behavior is on the border of what can be reliably estimated by this line shape analysis.

It is immediately clear upon inspection of Figs. 15 and 16 that the bridging ligand and the ancillary ligands play critical roles in determining the extent of electronic communication and the rates of electron transfer. First we will discuss the role of the ancillary ligands, which can be viewed in terms of energetic matching of ruthenium cluster dπ orbitals and bridging ligand π^* orbitals [9]. More electron donating pyridyl ligands contribute to greater electronic communication and faster electron transfer by raising the cluster orbital energies closer to LUMO of the bridging ligand, as well as by disfavoring redistribution of electron density onto the ancillary ligand itself.

The simple interpretation of the bridging ligand contribution is that the π^* orbitals of bipyridine lie well above those of pyrazine, and that the longer bipyridine reduces electronic communication

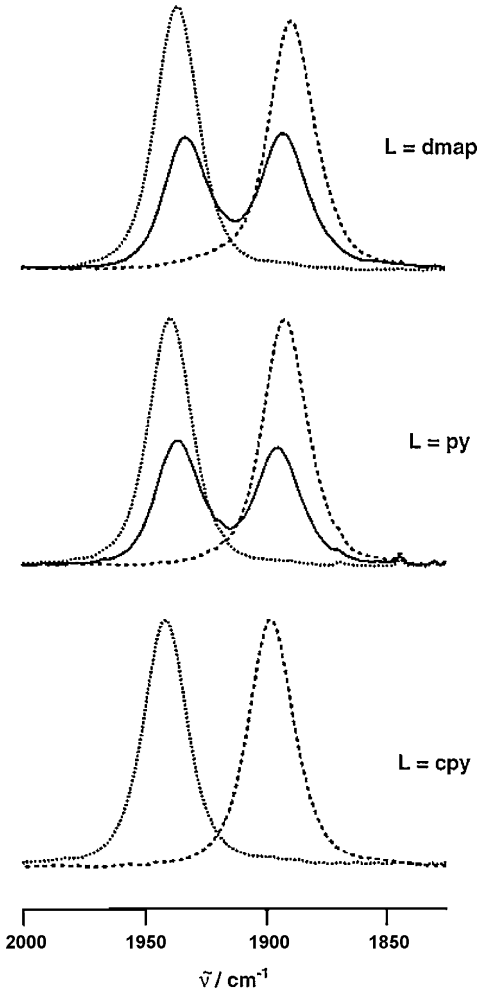

Fig. 15. Infrared spectra for bipyridine bridged complexes $[[Ru_3(\mu_3\text{-}O)(\mu\text{-}OAc)_6(CO)(L)]_2(\mu\text{-}bpy)]^n$ in CH_2Cl_2 with 0.1 M Bu_4NPF_6 ($n = 0$ (···), −1 (–), −2 (- - -)) [10].

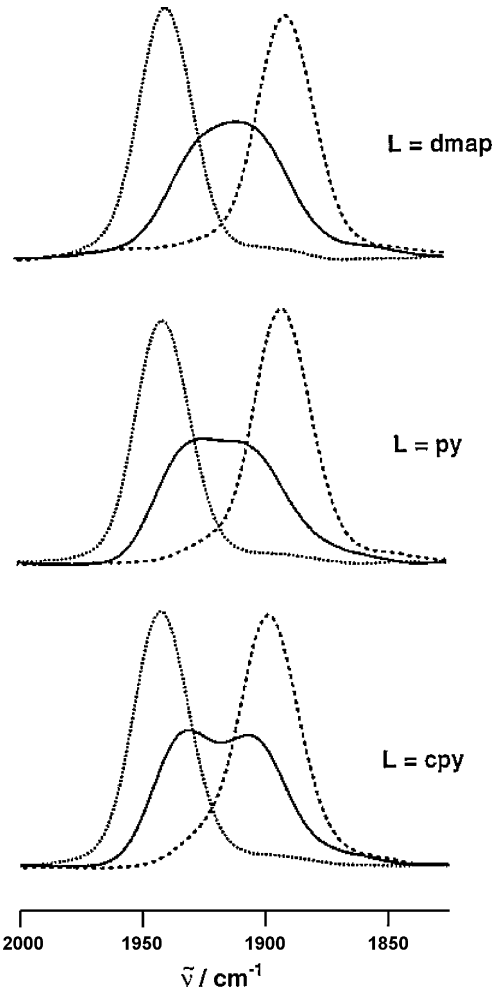

Fig. 16. Infrared spectra for pyrazine bridged complexes $[[Ru_3(\mu_3\text{-}O)(\mu\text{-}OAc)_6(CO)(L)]_2(\mu\text{-}pz)]^n$ in CH_2Cl_2 with 0.1 M Bu_4NPF_6 ($n = 0$ (···), −1 (–), −2 (- - -)) [10].

by increasing the electron transfer distance, which typically displays an exponential dependence [24,25]. As will be seen in the following sections, pyrazine vibrational modes and vibronic coupling also play important roles.

4. The bridge is rocking: entanglement of bridging ligand normal modes and intervalence transitions

Up to this point, we have seen two factors that distinguish intramolecular electron transfer in a mixed-valence ion from intermolecular self-exchange. They are (1) simple proximity and removing the requirement of diffusion for a donor/acceptor pair to exchange an electron; (2) energetic alignment of the donor-bridge-acceptor triad for optimal "resonant" exchange. Here we consider an additional important effect: the vibronic participation of bridging ligand normal modes. Electroabsorption [44] and resonance Raman [45] studies of the Creutz–Taube cation have shown that the description which best reflects spectroscopic observables is a valence averaged mixed-valence species described by the three-state vibronic coupling model where electronic states and vibrations of the bridging ligand and metal centers are explicitly included [46–48]. Because of the systematic variability in complexes **4**–**6**, insight can be gained with respect to the role of vibronic contributions of specific normal modes of the bridging pyrazine ligand as electronic communication is systematically adjusted in mixed-valence complexes that are nearly delocalized (Fig. 17). To

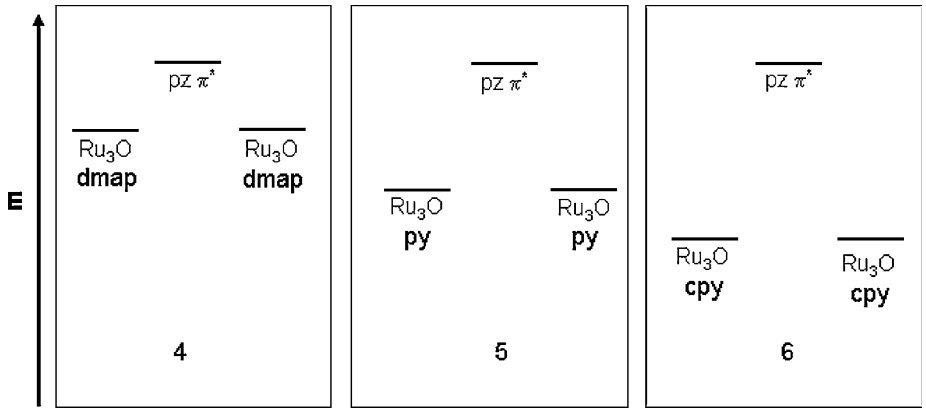

Fig. 17. Qualitative MO scheme showing relative energetic matching between ruthenium cluster dπ orbitals and pyrazine π* orbitals.

this end, **4**–**6** were interrogated by resonance Raman spectroelectrochemistry [15].

The resonance Raman experiment is a very powerful tool for studying vibronic coupling [49–51]. The experiment involves excitation of the IVCT band (or B → N transition, *vide infra*) of mixed-valence species and the detection of scattered light. Pertinent information taken from these experiments includes relative band energies and intensities of symmetric stretching modes of the bridging ligand. These symmetric modes for pyrazine are shown in Fig. 18.

Raman spectra of neutral **4**–**6** with an excitation wavelength of 752 nm reveal bands for neutral complexes at 1035, 1225, and 1605 cm^{-1} and are assigned to the ν_1, ν_{9a} and ν_{8a} modes of pyrazine, respectively. The excitation does not correspond to any of the electronic transitions observed in the neutral complex; however in the mixed-valence complexes it lies within the intervalence charge transfer band (IVCT) band. Upon one electron reduction, bands corresponding to symmetric modes are shifted to lower energy, at 1010, 1206, and 1584 cm^{-1}. This shift is consistent with a partial electronic occupation in the pyrazine π* orbital (LUMO) and indicates that this partial electronic occupation is an important contributor to the electronic character of the mixed-valence anions in $\mathbf{4}^-$–$\mathbf{6}^-$ [15]. This also lends more support to the idea that the strong coupling is due to significant unpaired electron density on the bridge (and that this can be controlled by varying the electron donor strength of the ancillary ligand). In addition to the shift in energy, all Raman bands exhibit increased integrated intensity due to the increased vibronic coupling of the bridging ligand symmetric vibrational modes to the IVCT transition.

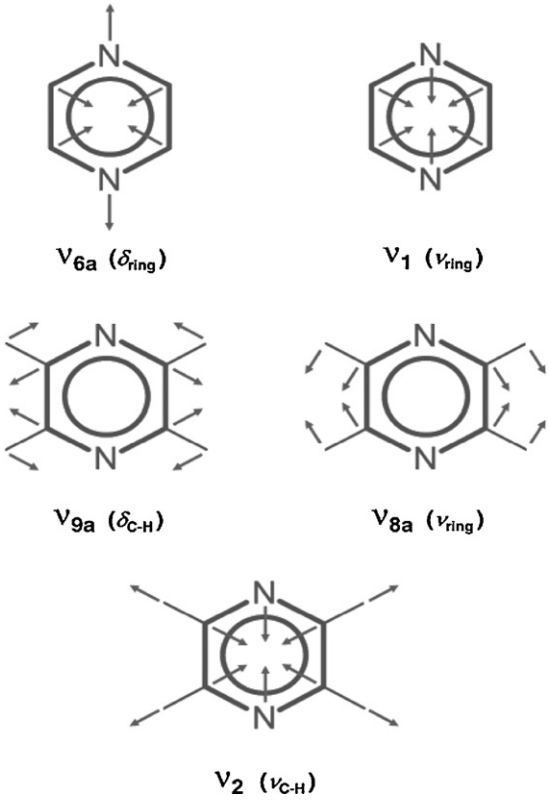

Fig. 18. Totally symmetric vibrational modes of pyrazine.

Greater enhancement of the symmetric pyrazine bands corresponds to greater electronic coupling through that pyrazine to the ruthenium clusters. Also, greater electronic occupancy of bridging ligand orbitals is expected to lead to more intense bridge-based Raman bands. The Raman enhancement is most pronounced in the ν_{8a} stretching mode, and indeed this mode showed greatest enhancement for the most electronically coupled species $\mathbf{4}^-$, relative to neutral **4**. This trend is consistent with increased comproportionation constants, faster estimated ET rates, and greater electronic coupling between Ru_3 clusters. Relative mode enhancements for mixed-valence anions are shown in Fig. 19 and summarized in Table 4.

The three-state model for mixed-valence complexes developed by Ondrechen and co-workers [46,47,52] can be used to describe the effects of vibronic coupling in $\mathbf{4}^-$–$\mathbf{6}^-$ [13]. As will be seen, predictions of the three-state model are consistent with the observed resonant enhancement of symmetric pyrazine modes upon excitation of the IVCT band in these mixed-valence complexes.

The three-state model assumes three electronic basis sets with parameterized interactions between them, and application of this to $\mathbf{4}^-$–$\mathbf{6}^-$ leads to three states that include two cluster band states and one bridge-based electronic state. Careful consideration of the electronic structure [53–55] along with DFT calculations of Ru_3O

Table 4
Summary of observed frequencies and relative peak intensities of resonant Raman spectra of **4**–**6** in the neutral and mixed-valence state [15].

Complex	Freq. (cm^{-1}), rel. intensity		
	Mode ν_1	Mode ν_{9a}	Mode ν_{8a}
$\mathbf{4}^0$	1033, 1.6	1223, 1.3	1604, 1.2
$\mathbf{4}^{-1}$	1007, 5.0	1205, 2.5	1587, 5.5
$\mathbf{5}^0$	1035, 0.75	1224, 0.60	1606, 0.65
$\mathbf{5}^{-1}$	1010, 4.4	1206, 1.5	1584, 2.6
$\mathbf{6}^0$	1035, 0.85	1226, 0.65	1605, 0.7
$\mathbf{6}^{-1}$	1008, 2.8	1206, 1.0	1580, 2.5

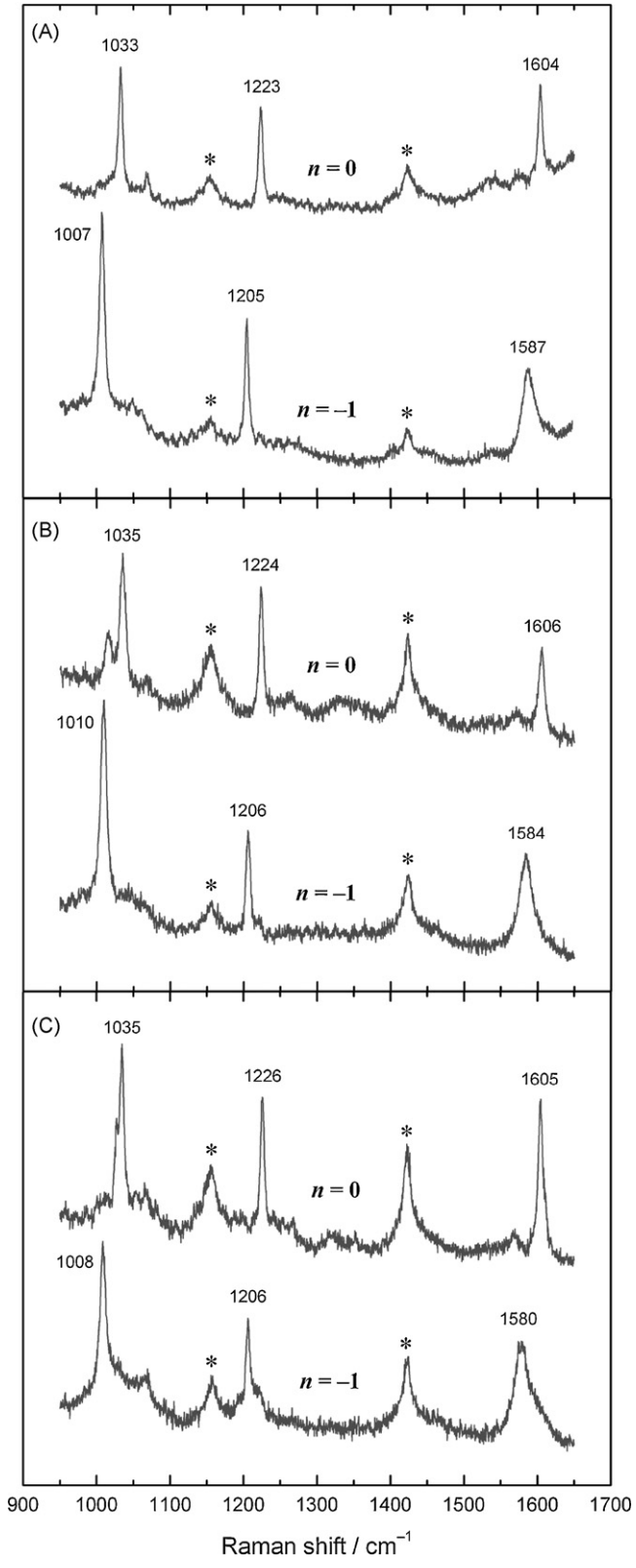

Fig. 19. Resonance Raman spectra of complexes **4** (a), **5** (b), and **6** (c) in the neutral (0) and mixed-valence (−1) states [15]. Solvent peaks are marked by an asterisk, and labeled peaks correspond to symmetric pyrazine modes.

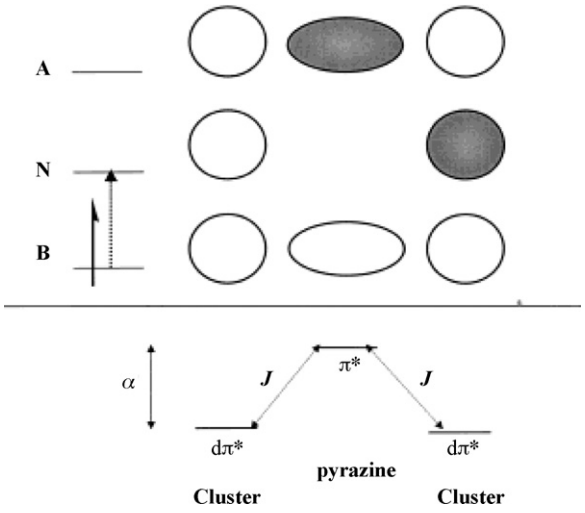

Fig. 20. Qualitative representation of molecular orbitals derived from the three-state model [13]. The B → N transition is the only symmetry allowed transition.

clusters show that the LUMO of the ruthenium cluster unit can be viewed as a dπ* orbital which is delocalized over the entire cluster. On the pyrazine bridging ligand, DFT and qualitative MO diagrams reveal that the orbital that best matches energy and spatial orbital overlap of the bound nitrogen position is an aromatic ring π* type molecular orbital [13]. From these molecular orbitals, a picture for the three-state model is formed where the unpaired electron can exchange between three sites; two where the electron is in a dπ* orbital on the cluster and one where the electron is in the higher energy π* orbital on the bridge (Fig. 20).

It is assumed that the two cluster-based states interact with one another through the bridge state, and the electronic parameters which describe this system are the exchange coupling between the cluster states and the bridge state, J, and the energy gap between the charge center states and the bridge state, α. Molecular orbitals constructed from this three-state model include bonding, non-bonding, and antibonding orbitals given by B, N, and A, respectively. In the ground state of the mixed-valence complex, the unpaired electron resides in the bonding orbital. Optical excitation of the mixed-valence complex leads to the intervalence transition, or in the three-state model, the symmetry allowed B → N transition. The energy of the transition is given by $E = (-1/2)\left(\alpha - \sqrt{(\alpha^2 8J^2)}\right)$ (with α and J defined above) and will reflect in large part the exchange coupling because of the relatively small energy difference between pyrazine and cluster basis sets [13]. Because there is a node in the N electronic state, the B → N transition has the character of a pyrazine to two-cluster charge transfer, or more simply, LMCT. It is expected that a B → N transition will involve a large nuclear rearrangement in the case of the bridging ligand as the electronic occupation of the π* orbital changes. It is this action that explains the observed vibronic coupling between a B → N transition and the symmetric pyrazine vibrational modes. Also verified by this picture is the shift to lower energy of the symmetric pyrazine modes in the mixed-valence state as compared to the isoelectronic (neutral) state. The three-state description also elucidates the enhancement of symmetric stretching modes. The degree to which charge is transferred between the bridge and the clusters will control the displacement of the ground and excited state surfaces from one another along the vibrational (geometrical) coordinates. As the displacement increases, one expects to observe an enhancement of vibronic coupling [51], as depicted in Fig. 21. Important modes derived from the three-state model that contribute to charge transfer are shown in Fig. 22 [13].

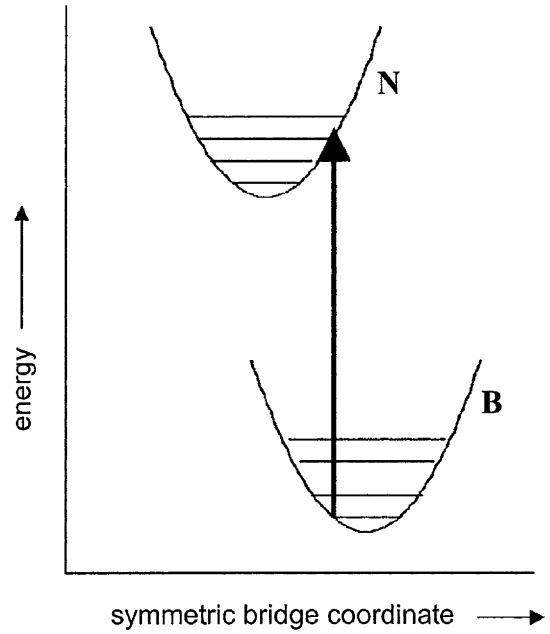

Fig. 21. Vibronic coupling of a symmetric bridge vibration to the B → N electronic transition [13]. Because the transition involves partial electron transfer from the bridging ligand clusters, there is a significant shift along the symmetric coordinate between the minima for the ground (B) and excited (N) electronic states.

The take-home message from this picture is that the most important modes to consider in bridged ET are those modes that vary the bond length between the bridging ligand and the two charge-sites. These modes are the most enhanced in the resonance Raman, indicating that the potential energy surfaces involved in the IVCT are most strongly offset along these coordinates. In other words, it is along these coordinates that the ET sees the greatest reorganizational barrier. In the case of a pyrazine bridge, these modes are the ν_1, ν_{9a} and ν_{8a}, which display the greatest vibronic enhancement.

An extension of the three-state model which is perhaps a more complete description of vibronic coupling in the dimer of ruthenium trimer systems is a five-state model where energies and molecular orbitals of ancillary pyridyl ligands are explicitly

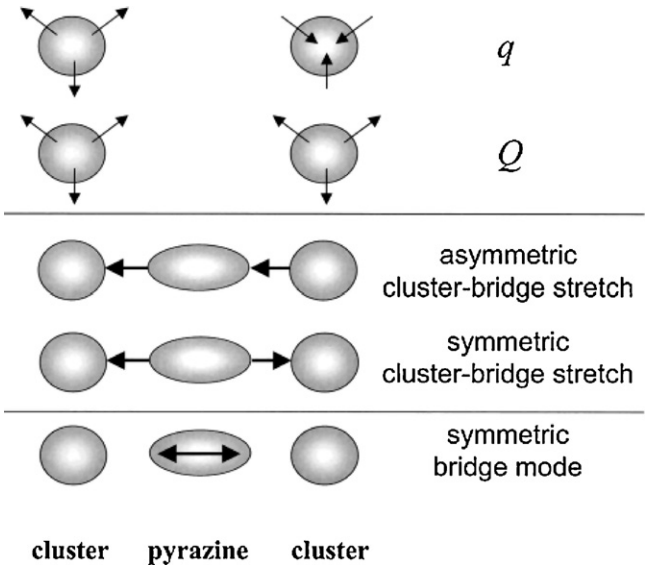

Fig. 22. Important modes of the three-state model which contribute to electron transfer [13].

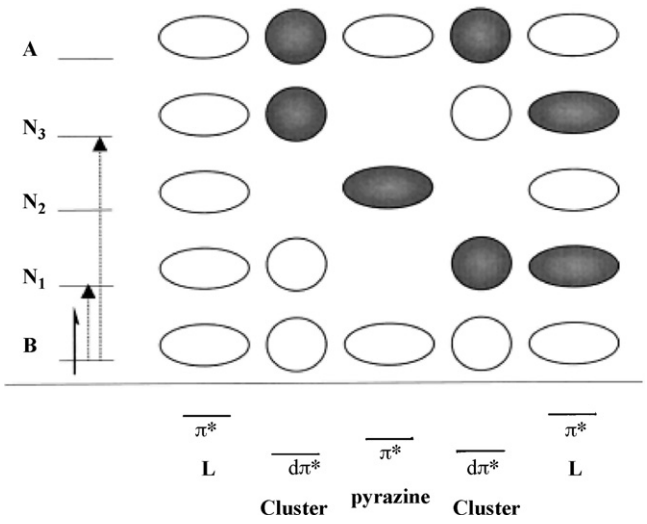

Fig. 23. Qualitative molecular orbitals of a five-state model for electronic delocalization in **4**⁻–**6**⁻, with electronic occupation expected for the (−1) mixed-valence species [13]. Energy gaps between states and relative energies of states are not necessarily accurate due to possible energy gap effects. Two symmetry-allowed electronic transitions for the single electron are expected: B → N_1 and B → N_3. Relative energies are not necessarily to scale.

included. DFT calculations on a monomeric ruthenium cluster with two pyridyl ligands, complex **2**, confirms substantial coupling between the ligands and the cluster, where a low lying pπ* orbital on the pyridine interacts with the dπ* metal center orbitals of the cluster to form a molecular orbital spanning the entire complex [13]. If an exchange coupling interaction between ancillary pyridine ligands and Ru_3 cluster is of the same order of magnitude as the [dπ*(cluster) ↔ π*(pyrazine)] interaction, then the delocalization of a single electron in the three-state model would be more completely described by a five-state/five-center model inclusive of the pπ* orbitals on the ancillary ligands. The qualitative molecular orbital diagram predicted by a five-state model is shown in the lower part of Fig. 23.

The orbitals and electronic behavior of the mixed-valence electronic transition are not greatly different from the three-state model. The system is still described by single electronic occupation in the mixed-valence state, and the ground electronic state is still a fully symmetric bonding type molecular orbital. There are two allowed electronic transitions in this scheme, B → N_1 and B → N_3, both of which have the same properties of the B → N transition from the three-state model. In particular, the electronic excited states each have a node on the bridging ligand and as such the transitions are expected to be partially LMCT in character rather than MMCT in character. We can think of this departure from the three-state model as a split in energy of the B → N transition by electron exchange interaction with pyridyl ligand π* levels, and the N_1 and N_3 molecular orbitals are in essence symmetric and antisymmetric combination of the N molecular orbital from the three-state model.

Predictions from the five-state electronic model are consistent with the observed near infrared spectra of mixed-valence complexes **4**⁻–**6**⁻, which have two bands at approximately 7000 cm^{-1} and 12,000 cm^{-1}. It would seem from the five-state model that the B → N_1 and B → N_3 transitions are both a part of the IT transition. Firm spectral evidence in support of the five-state model requires resolution of overlapping of pyrazine bridging modes and pyridine modes. Not unexpectedly, because of their similarity in structure, pyridyl ligands and pyrazine have nearly coincident vibrational frequencies. It was initially a challenge to assign which pyridine and pyrazine modes were aiding resonant enhancement in Raman spectra. Resonant Raman experiments were performed

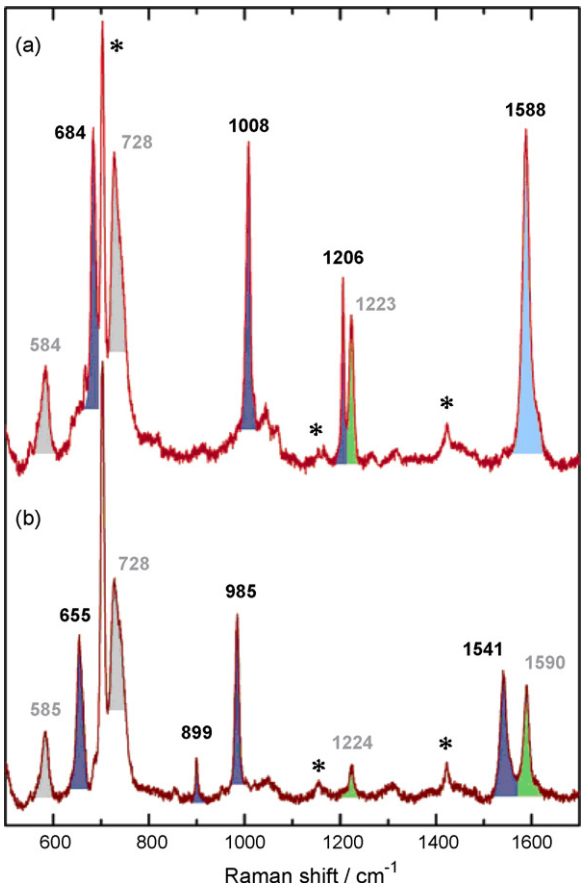

Fig. 24. Resonance Raman spectra of (a) $\mathbf{4}^-$ (pz-h_4) and (b) $\mathbf{4}^-$ (pz-d_4) [13]. Solvent peaks (methylene chloride) are marked by asterisks. The shading colors represent the assignments in terms of molecular fragments, as follows: blue, bridging pz; green, peripheral dmap; cyan, bridging pz + peripheral dmap; gray, cluster core Ru_3O.

on the mixed-valence anion of **4** where the pyrazine-h_4 bridge had been substituted with a pyrazine-d_4 bridge [6]. Deuteration shifts frequencies of the pyrazine modes to lower energies, allowing resolution of pyridyl and pyrazine modes, shown in Fig. 24.

What becomes clear from this investigation is that two modes on peripheral rings were involved; the ν_{8a} and ν_{9a} modes on the 4-dimethylaminopyridine (dmap) ligand. Furthermore, comparison to solvent intensities (which remain constant throughout the experiment) confirmed resonant enhancement of these two dmap modes in the mixed-valence state. This vibronic involvement of the ancillary ligands supports the five-state/five-center model for $\mathbf{4}^-$–$\mathbf{6}^-$ mixed-valence complexes. Additionally, from the study of deuterated pyrazine dmap dimer, vibrational modes involving both μ-oxo-bridged trinuclear cluster (Ru_3O) core and metal–cluster–ligand framework (Ru–N_{ring}) were resolved in resonance Raman spectra. All of these taken together clearly indicate that all molecular fragments of the five-state model are coupled to the "intervalence" charge transfer in the mixed-valence anion.

The IVCT resonance Raman spectra of nearly delocalized mixed-valence systems show very satisfactory agreement with the three-state model and excellent agreement with the five-state model. The utility of intervalence-resonant Raman spectroscopy in exploring the importance of vibronic coupling in localized to delocalized transition in mixed-valence chemistry is emphasized by this work. Excellent evidence is provided for the vibronic coupling of totally symmetric bridging pyrazine vibrations to the B → N transitions. Results described herein are broadly applicable to a greater

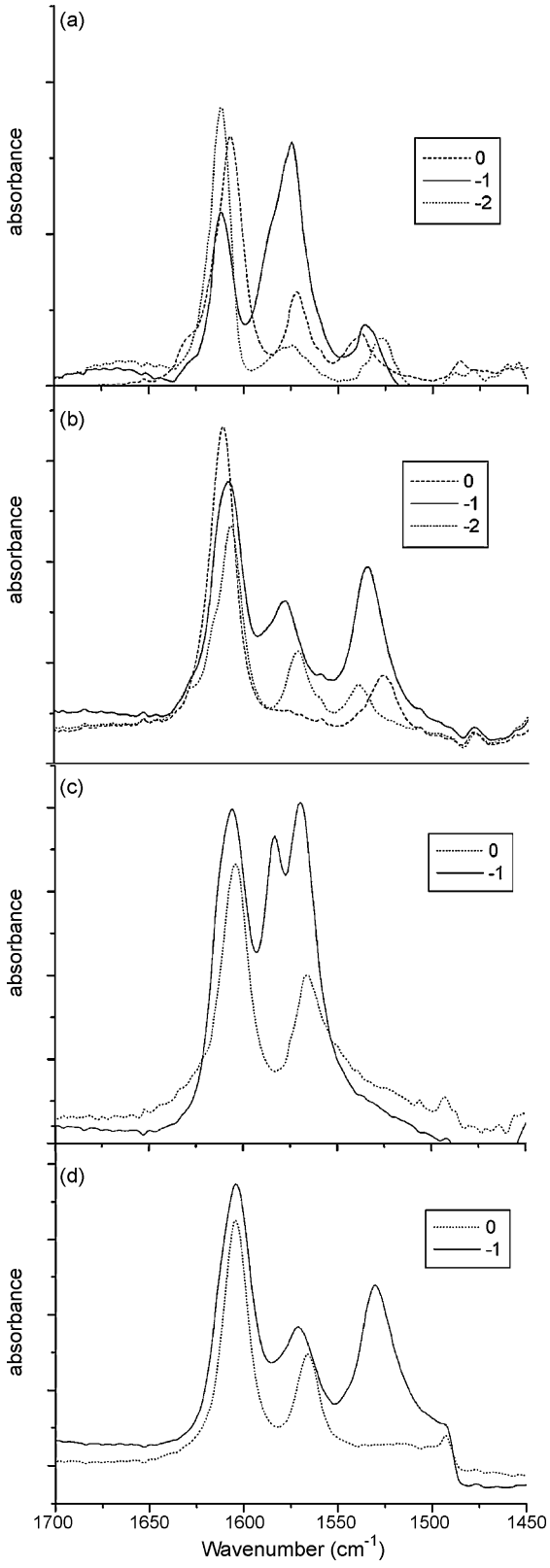

Fig. 25. Infrared spectroelectrochemistry of the region 1500–1700 cm^{-1} of: (a) **4** in the (0), (−1) and (−2) oxidation states, (b) **4** where the bridge has been substituted with pz-d_4 in the (0), (−1) and (−2) oxidation states, (c) **6** in the (0) and (−1) oxidation state and (d) **6** where the bridge has been substituted with pz-d_4 in the (0) and (−1) oxidation state [5].

understanding of general dynamic electron transfer phenomena and mixed-valence behavior in the nearly delocalized regime.

5. If the bridge is rocking, the IR can be shocking

The significant enhancements of totally symmetric pyrazine modes of vibration seen in the resonance Raman spectroscopy of the mixed-valence ions $\mathbf{4}^-$–$\mathbf{6}^-$ are explained well by vibronic involvement of these modes in the IVCT electronic transition. A second, somewhat less obvious result of strong vibronic coupling is the appearance of totally symmetric pyrazine modes in IR spectra. The vibronic enhancement of normally forbidden IR transitions is distinctly different from the use of the ν_{8a} mode as a marker for localization of charge on the time scale longer than the period of the mode, ca. 20 fs [23,56]. IR activity of symmetric pyrazine modes exists in the full IR spectra for mixed-valence anions $\mathbf{4}^-$–$\mathbf{6}^-$, but the active ν_{8a} mode (the most intense of these bands) in particular is overlapped with cluster acetate bands and is not unambiguously clear. Isotopic labeling of pyrazine hydrogens with deuterium shifts the frequency of the ν_{8a} mode to avoid this overlap. As can be seen from Fig. 25, the ν_{8a} mode of the labeled pyrazine appears at 1535 cm^{-1} in complex **4** pz-d_4.

Comparable frequency shifts in complexes **4**–**6** are also observed. In free pyrazine, the ν_{8a} mode is of A_g symmetry and is not IR active. It is important to note that when each Ru_3O cluster is electronically equivalent, in the (0) and (−2) states, the ν_{8a} mode is inactive. In the (−1) state there exists an inequivalency between the two clusters which effectively breaks the electronic symmetry of the molecule and could lead to activation of this particular mode. Of consequence is the fact that very little difference in extinction coefficients for the ν_{8a} band is observed in $\mathbf{4}^-$–$\mathbf{6}^-$ which suggests two things. First, the origin of IR activity in each of the mixed-valence complexes is qualitatively the same. Second, if the origin of the infrared intensity is vibronic, then there is very little difference between the vibronic coupling constants for complexes with different strengths of electronic communication. Perhaps even more telling is a comparison to non-mixed-valence complexes with intentionally asymmetric coordination environments about the pyrazine. In SEC of mixed-valence asymmetric dimer complexes (where ancillary L1 ≠ L2) an identical pattern is seen: the ν_{8a} mode is only active in the (−1) state. The fact that there is no IR activity of ν_{8a} mode in isovalent states of complexes that contain deliberate and substantial asymmetries indicates that asymmetry about the pyrazine does not lead to strong IR activity in the symmetric ν_{8a} band of $\mathbf{4}^-$–$\mathbf{6}^-$. In a more extremely asymmetric environment where pz is an η^1 ligand in a monomeric species $\{Ru_3O(OAc)_6(L)(\eta^1\text{-pz-}d_4)\}$, one pz nitrogen is bound to the Ru cluster and the other is not. In the neutral state, the ν_{8a} exhibits only very weak IR activity, however in the (−1) state it shows strong activity and is shifted to a much lower frequency. This effect confirms that pronounced enhancement of the IR activity of the symmetric mode cannot be due to electronic localization longer than one period of the ν_{8a} vibration. What does explain this phenomenon is the following. In the monoanionic state of the monomeric species, the unpaired electron is expected to experience significant stabilization through exchange coupling via the orbital overlap of the $d\pi^*$ orbital of the cluster and the π^* orbital on the pyrazine. Extending this to $\mathbf{4}^-$–$\mathbf{6}^-$, it is likely that strong infrared activity in otherwise weak or symmetry-forbidden normal modes appears to be one of the vibronic consequences of this significant mixing of adjacent pyrazine and cluster-based electronic sites.

6. Solvent freezes before bridge: the role of solvent dynamics

Within the Robin–Day classification scheme for mixed-valence complexes, microscopic descriptions have evolved for Class II and Class III systems in solution. In a Class II system, the solvent and exchanging electron are localized; while in a Class III system, the solvent and exchanging electron are averaged. A question of particular interest in mixed valency is where exactly does the localized to delocalized transition occur, and how can you tell?

In nearly delocalized mixed-valence complexes, the energetic barrier to intramolecular electron transfer is close to zero, which means the rate of ET will depend largely on the preexponential nuclear frequency factor, ν_N. In solution, ν_N is governed by solvent frequencies and intramolecular vibrations, and of these the solvent dynamics are expected to be the major contributor, as they are slower than internal vibrations. We know from reso-

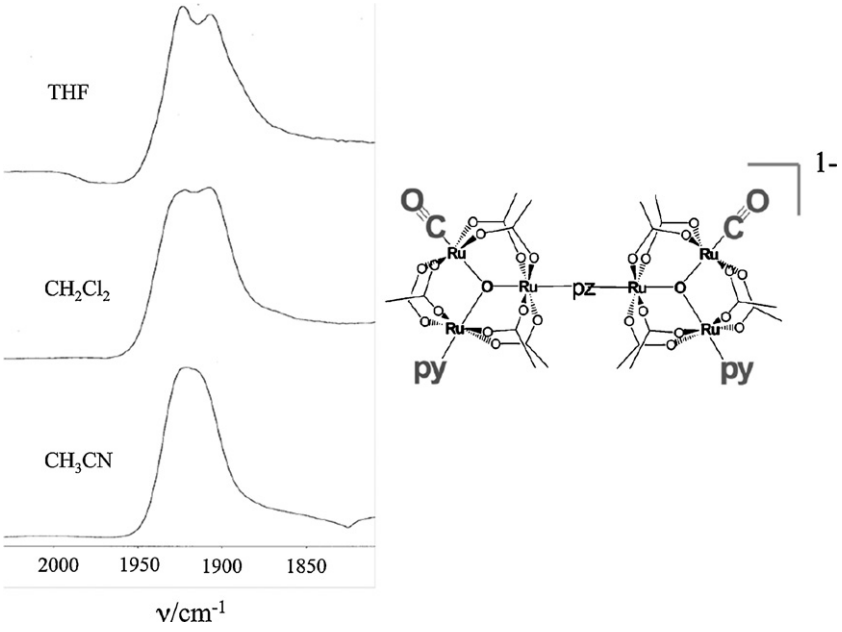

Fig. 26. IR band shapes for the ν(CO) band of $\mathbf{5}^-$ in THF, CH_2Cl_2, and CH_3CN. More coalesced spectra are associated with faster electron-transfer rates.

nance Raman studies that electron transfer is mediated in part by the ν_{8a} symmetric stretching frequency of the pyrazine bridging ligand. The frequency of this vibration is $4.8 \times 10^{13}\ s^{-1}$, while the fastest solvent dipolar reorientation frequency of the solvents studied by Maroncelli is $6.7 \times 10^{12}\ s^{-1}$ (for acetonitrile) [57]. These simple considerations help define the timeframe for the localized to delocalized transition at the Class II/III borderline. First, the vibrational modes that are important in ET and contribute to the pre-exponential frequency factor determine the upper limit in rate of a delocalized system. Second, when the activation barrier for ET is near zero, it may be impossible for a system to fully delocalize at the fastest time scale because (slower) solvent frequencies cannot keep pace. It is clear that a localization/delocalization boundary can exist between these two limits.

It can be seen from Fig. 26 that ν(CO) bandshapes of the mixed-valence dimer **5**$^-$ depend on solvent, and that the bandshape is much more coalesced in acetonitrile than in THF. Simulation gives intramolecular ET rate constants of $1.1 \times 10^{12}\ s^{-1}$, $1.8 \times 10^{12}\ s^{-1}$, and $2.6 \times 10^{12}\ s^{-1}$ in tetrahydrofuran, methylene chloride and acetonitrile, respectively. Such dependences of ET rates on solvent are usually explained well by considering the solvent reorganization energies, i.e. the energetic contribution of the solvent to the barrier, Eq. (3):

$$\lambda_0 = \frac{(\Delta e)^2}{8\pi}\left(\frac{1}{\varepsilon_{op}} - \frac{1}{\varepsilon_s}\right)\int (D_A - D_B)^2\, d\tau \qquad (3)$$

Here Δe is the charge transferred, ε_{op} is the optical dielectric constant, ε_s is the static dielectric constant, and D_A and D_B are the dielectric displacement vectors of the precursor and successor complexes, respectively.

Electron transfer properties of **4**$^-$–**6**$^-$ were probed in seven different organic solvents, and rates of electron transfer were correlated with thermodynamic and dynamic solvent parameters [4]. Our investigation showed that rates of electron transfer correlated poorly with outer sphere solvent reorganization energies, microscopic solvent polarities, static dielectric constants, and optical dielectric constants—all thermodynamic and largely time independent solvent parameters. This result shows that as the barrier to electron transfer approaches zero, the solvent reorganizational contribution to the barrier becomes unimportant. Examination of time *dependent* solvent parameters revealed strong correlation to rates of ET in **4**$^-$–**6**$^-$, most notably the solvent dipolar reorientation frequencies [57]. This study illustrates that solvent *dynamics* significantly influence rates of ET in the ground states of nearly delocalized mixed-valence complexes. The dependence of k_{ET} on solvent dynamical processes that occur at or near the picosecond time scale was a key finding for us for several reasons. First, it lends some validity to the use of 1D IR lineshapes to estimate k_{ET} values on the order of 1 ps^{-1} since these rate constants are so strongly affected by solvent dynamical processes that are known to occur on the same time scale. Second, it raises the question about whether such systems would still show evidence of localization (i.e. two peaks in the ν(CO) IR spectra in tetrahydrofuran and methylene chloride in Fig. 26) if solvent dynamics were not so much in play. One way to partially arrest solvent motion and probe this question is to freeze the solvent [20].

Spectra in Fig. 27 show ν(CO) bands for mixed-valence ion **6**$^-$ in two different solvents at increasingly colder temperatures. From these spectra it is clear that as the temperature decreases, spectral coalescence increases until the solvent is frozen. Beyond the freezing point the bandshapes do not change (i.e. rates of ET remain the same). Also, comparison of ν(CO) bandshapes for **6**$^-$ in frozen methylene chloride and frozen acetonitrile solutions show that once the two different solvents have frozen, the rates of electron transfer are the same. These results demonstrate a localized to delocalized transition at the freezing point, where solvent dynamics become largely uncoupled from electron transfer and internal vibrational modes of the molecule dominate ν_N. It appears that for Class II and Class III borderline mixed-valence systems, a fluid solvent imposes a "speed limit" for electron transfer.

This study captures a more complete picture of mixed valency at the Class II/III borderline. Rates of intramolecular electron transfer in nearly delocalized systems are highly dependent on solvent dynamic parameters and *not* solvent thermodynamic parameters such as the solvent reorganization energy or solvent polarity (which were seen to affect the much slower intermolecular ET between monomers in the NMR study above), and it is clear that in this limit the solvent motion does not appear *averaged* to the exchanging electron, but limits in a motional sense how fast the electron can exchange. A precise definition of Class II/III mixed-valence complexes that follows from this research is that the solvent dynamical

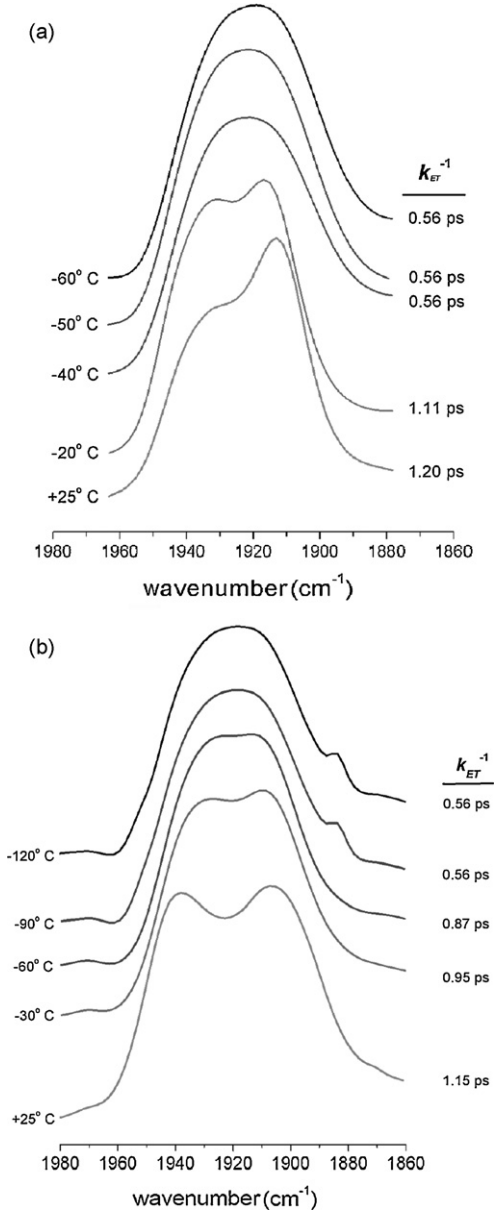

Fig. 27. IR band shapes for ν(CO) of the mixed-valence dimer **6**$^-$ in CH_3CN (top) and CH_2Cl_2 (bottom) as a function of temperature [20]. The band shape shows increasing coalescence as the freezing point of the solution is approached. To the right of each spectrum are listed the electron-transfer lifetimes obtained from simulation of that spectrum.

parameters control rates of ET in borderline systems, and tend to localize otherwise delocalized electronic states.

7. Maintaining the bridge to the 21st century

In this review, we have highlighted some of our efforts from the past 12 years towards a more complete understanding of mixed valency. Oxo-centered ruthenium acetate trimers have proven so versatile that they have revealed interesting behaviors in intermolecular self-exchange reactions and intramolecular electron transfer at the Robin–Day Class II/III border. We have probed the role of orbital overlap in intermolecular electron transfer, as well as in intramolecular ETs that are so fast that the usual analysis of solvent effects no longer applies. Perhaps most importantly the work provides a new definition of the Class II and Class III border, where solvent dynamical parameters control rates of ET when activation energies approach zero.

Acknowledgments

We gratefully acknowledge support from NSF for this work. We also acknowledge many years of enjoyable and productive collaboration with Prof. Tasuku Ito (now retired) of Tohoku University, Sendai, Japan.

References

[1] B.K. Breedlove, T. Yamaguchi, T. Ito, C.H. Londergan, C.P. Kubiak, Compr. Coord. Chem. II 2 (2004) 717.
[2] J.C. Goeltz, C.P. Kubiak, J. Phys. Chem. C 112 (2008) 8114.
[3] T. Ito, N. Imai, T. Yamaguchi, T. Hamaguchi, C.H. Londergan, C.P. Kubiak, Angew. Chem. Int. Ed. 43 (2004) 1376.
[4] B.J. Lear, S.D. Glover, J.C. Salsman, C.H. Londergan, C.P. Kubiak, J. Am. Chem. Soc. 129 (2007) 12772.
[5] C.H. Londergan, J.C. Salsman, S. Ronco, C.P. Kubiak, Inorg. Chem. 42 (2003) 926.
[6] R.C. Rocha, M.G. Brown, C.H. Londergan, J.C. Salsman, C.P. Kubiak, A.P. Shreve, J. Phys. Chem. A 109 (2005) 9006.
[7] J.C. Salsman, C.P. Kubiak, in: W. Kaim, A. Klein (Eds.), Spectroelectrochemisty, Royal Society of Chemistry, Cambridge, 2008, p. 123.
[8] J.C. Salsman, C.P. Kubiak, T. Ito, J. Am. Chem. Soc. 127 (2005) 2382.
[9] J.C. Salsman, S. Ronco, C.H. Londergan, C.P. Kubiak, Inorg. Chem. 45 (2006) 547.
[10] T. Ito, T. Hamaguchi, H. Nagino, T. Yamaguchi, H. Kido, I.S. Zavarine, T. Richmond, J. Washington, C.P. Kubiak, J. Am. Chem. Soc. 121 (1999) 4625.
[11] T. Ito, T. Hamaguchi, H. Nagino, T. Yamaguchi, J. Washington, C.P. Kubiak, Science (USA) 277 (1997) 660.
[12] B.J. Lear, C.P. Kubiak, Inorg. Chem. 45 (2006) 7041.
[13] C.H. Londergan, C.P. Kubiak, J. Phys. Chem. A 107 (2003) 9301.
[14] C.H. Londergan, C.P. Kubiak, Chem.-Eur. J. 9 (2003) 5962.
[15] C.H. Londergan, R.C. Rocha, M.G. Brown, A.P. Shreve, C.P. Kubiak, J. Am. Chem. Soc. 125 (2003) 13912.
[16] C.H. Londergan, J.C. Salsman, B.J. Lear, C.P. Kubiak, Chem. Phys. 324 (2006) 57.
[17] C.H. Londergan, J.C. Salsman, S. Ronco, L.M. Dolkas, C.P. Kubiak, J. Am. Chem. Soc. 124 (2002) 6236.
[18] K. Ota, H. Sasaki, T. Matsui, T. Hamaguchi, T. Yamaguchi, T. Ito, H. Kido, C.P. Kubiak, Inorg. Chem. 38 (1999) 4070.
[19] T. Yamaguchi, N. Imai, T. Ito, C.P. Kubiak, Bull. Chem. Soc. Jpn. 73 (2000) 1205.
[20] S.D. Glover, B.J. Lear, J.C. Salsman, C.H. Londergan, C.P. Kubiak, Philos. Trans. R. Soc. A 366 (2008) 177.
[21] J.C. Goeltz, C.J. Hanson, C.P. Kubiak, Inorg. Chem. 48 (2009) 4763.
[22] M.B. Robin, P. Day, Adv. Inorg. Chem. Radiochem. 10 (1967) 247.
[23] K.D. Demadis, C.M. Hartshorn, T.J. Meyer, Chem. Rev. 101 (2001) 2655.
[24] N.S. Hush, Prog. Inorg. Chem. 8 (1967) 391.
[25] R.A. Marcus, Annu. Rev. Phys. Chem. 15 (1964) 155.
[26] D.M. Stanbury (Ed.), Nuclear Factors in Main-group Electron Transfer Reactions, 1997.
[27] S.F. Nelsen, R.F. Ismagilov, K.E. Gentile, M.A. Nagy, H.Q. Tran, Q.L. Qu, D.T. Halfen, A.L. Odegard, J.R. Pladziewicz, J. Am. Chem. Soc. 120 (1998) 8230.
[28] M.-S. Chan, J.B. DeRoos, A.C. Wahl, J. Phys. Chem. 77 (1973) 2163.
[29] J. Coddington, S. Wherland, Inorg. Chem. 36 (1997) 6235.
[30] J.L. Walsh, J.A. Baumann, T.J. Meyer, Inorg. Chem. 19 (1980) 2145.
[31] R.M. Nielson, M.N. Golovin, G.E. McManis, M.J. Weaver, J. Am. Chem. Soc. 110 (1988) 1745.
[32] R.M. Nielson, G.E. McManis, M.N. Golovin, M.J. Weaver, J. Phys. Chem. 92 (1988) 3441.
[33] B.A. Kowert, M.J. Fehr, P.J. Sheaff, Inorg. Chem. 47 (2008) 5696.
[34] E.S. Yang, M.S. Chan, A.C. Wahl, J. Phys. Chem. 79 (1975) 2049.
[35] C.J. Ballhausen, H.B. Gray, Molecular Orbital Theory, 1st ed., Benjamin, New York, 1965.
[36] B.S. Brunschwig, C. Creutz, N. Sutin, Chem. Soc. Rev. 31 (2002) 168.
[37] R. Delarosa, P.J. Chang, F. Salaymeh, J.C. Curtis, Inorg. Chem. 24 (1985) 4229.
[38] D.E. Richardson, H. Taube, Inorg. Chem. 20 (1981) 1278.
[39] D.E. Richardson, H. Taube, Coord. Chem. Rev. 60 (1984) 107.
[40] J.E. Sutton, H. Taube, Inorg. Chem. 20 (1981) 3126.
[41] Y.H. Dong, J.T. Hupp, Inorg. Chem. 31 (1992) 3170.
[42] M. Lacoste, H. Rabaa, D. Astruc, N. Ardoin, F. Varret, J.Y. Saillard, A. Lebeuze, J. Am. Chem. Soc. 112 (1990) 9548.
[43] F.W. Grevels, K. Kerpen, W.E. Klotzbucher, R.E.D. McClung, G. Russell, M. Viotte, K. Schaffner, J. Am. Chem. Soc. 120 (1998) 10423.
[44] D.H. Oh, M. Sano, S.G. Boxer, J. Am. Chem. Soc. 113 (1991) 6880.
[45] H. Lu, V. Petrov, J.T. Hupp, Chem. Phys. Lett. 235 (1995) 521.
[46] M.J. Ondrechen, J. Ko, L.-T. Zhang, J. Am. Chem. Soc. 109 (1987) 1672.
[47] L.T. Zhang, J.J. Ko, M.J. Ondrechen, J. Phys. Chem. 93 (1989) 3030.
[48] A. Ferretti, A. Lami, M.J. Ondrechen, G. Villani, J. Phys. Chem. 99 (1995) 10484.
[49] R.J.H. Clark, T.J. Dines, Angew. Chem. Int. Ed. 25 (1986) 131.
[50] A.B. Myers, Chem. Rev. 96 (1996) 911.
[51] J.T. Hupp, R.D. Williams, Acc. Chem. Res. 34 (2001) 808.
[52] L.T. Zhang, J. Ko, M.J. Ondrechen, J. Am. Chem. Soc. 109 (1987) 1666.
[53] J.A. Baumann, D.J. Salmon, S.T. Wilson, T.J. Meyer, Inorg. Chem. 18 (1979) 2472.
[54] J.A. Baumann, S.T. Wilson, D.J. Salmon, P.L. Hood, T.J. Meyer, J. Am. Chem. Soc. 101 (1979) 2916.
[55] F.A. Cotton, J.G. Norman, A. Spencer, G. Wilkinson, J. Chem. Soc. D: Chem. Commun. (1971) 967.
[56] R.C. Rocha, A.P. Shreve, Chem. Phys. 326 (2006) 24.
[57] M.L. Horng, J.A. Gardecki, A. Papazyan, M. Maroncelli, J. Phys. Chem. 99 (1995) 17311.